Vibration Assignment, B3pw91 Calculation and Conformational Analysis of Antimicrobial 5-Amino -3-(Methylthio)-1-(1,3,4-Thiadiazol -2-Yl)-1H-Pyrazole-4-Carbonitrile.

Medhat Mohamed El-Moselhy[1], Usama. A. Soliman[1*], H. G. Mohamedbakr[1], Mohamed S. Thabet[1], Mahmoud M. Abdelall[2], Ali M. Hassan[2]

[1]Department of Physical Sciences, Chemistry Division, College of Science, Jazan University, P.O. Box. 114, Jazan 45142, Kingdom of Saudi Arabia

[2]Department of Chemistry, College of Science, Al-Azhar University (Men's Campus), Nasr City 11884, Cairo, Egypt.

Abstract: In this study, we conducted infrared spectroscopy measurements on solid 5-amino-3-(methylthio)-1-(1,3,4-thiadiazol-2-yl)-1H-pyrazole-4-carbonitrile (AMTDPC, $C_7H_6N_6S_2$). The spectra were obtained at a resolution of 4 cm^{-1} and 0.5 cm^{-1}, within the spectrum region of 4000–200 cm^{-1}. Furthermore, the observation of NMR spectra for ^1H and ^{13}C has been documented. Nine rotational isomerisms, consisting of nine Cs and one C1 symmetry, are postulated for the AMTDPC molecule due to internal rotation occurring around C–N and/or C–S bonds. The isomers are finally characterized by two conformers (1-2) with energies below 1000 cm^{-1}, as determined through quantum mechanical calculations utilizing RHF and DFT/B3PW91. Based on forecasts, conformer 1, which is the rotamer with the lowest energy and produces real frequencies, is expected to have a stability order of 1 > 2. The spectrum modeling provides complete support for Conformer 1, making it the preferred option based on the recorded infrared (IR), ^1H, and ^{13}C spectral data. The chemical shifts at the B3PW91/6-31G level were successfully determined using the Polarizable Continuum Model (PCM) and the Gauge-Invariant Atomic Orbitals (GIAO) technique, regardless of the presence or absence of the solvent. The results of the NMR studies provided indications of both constrained and unconstrained internal rotation of NH_2 around C-N bonds. In order to propose a comprehensive and reliable vibrational assignment for each of the foundations of AMTDPC, potential energy distributions and normal coordinate analysis have been employed. Additionally, supplementary investigations were carried out to examine the torsional obstacles encountered during the internal rotation of the NH_2, CH_3, CH_3S, and thiadiazole ring. Based on spectrum measurements that exhibited a high level of concurrence with the anticipated values, it may be concluded that conformer 1 emerged as the isomer with the highest stability. Also there are small differences between the calculated bond distances and the x-ray readings for comprised compounds.

Keywords*:* Conformational durability, vibrational categorization, NMR profiles, standard coordinate assessment, obstacles to inner rotation, and computational estimations using DFT.

***Corresponding author:**
Assistant Professor, Department of Physical Sciences, Chemistry Division, College of Science, Jazan University, P.O. Box. 114, Jazan 45142, Kingdom of Saudi Arabia, Tel: +966-535092495; e-mail: usoliman@jazanu.edu.sa

تخصيص الاهتزاز، حساب B3PW91 وتحليل الهيكل لمضادات الميكروبات 5-أمينو -3-(ميثيلثيو)-1-(4،3،1-ثياديازول -2-إيل)- 1-Hبيرازول-4-كربونايتريل.

الملخص: تم قياس الطيف الأشعة تحت الحمراء للمركب الصلب 5-أمينو-3-(ميثيلثيو)-1-(4،3،1-ثياديازول-2-إيل)-1-Hبيرازول-4-كربونايتريلAMTDPC) ، (C7H6N6S2 في نطاق الطيف من 4000 إلى 200 سم$^{-1}$ بدقة 4 و 0.5 سم$^{-1}$ على التوالي. وقد تم أيضًا تسجيل طيفي الرنين النووي المغناطيسي البروتوني (1H) والكربوني-13 .(13C) نتيجة للدوران الداخلي حول روابط C–N و/أوC–S، تم اقتراح تسعة من الأيزومريات الدورية لجزيء) AMTDPC بتناظر Cs وتناظر .(C1 باستخدام حسابات الكم ا RHF وDFT/B3PW91 ، تم التوصل إلى وجود تلك الأيزومريات على شكل تآلفين (1-2) بطاقات طاقة أقل من 1000 سم$^{-1}$. تم التنبؤ بترتيب الاستقرار ليكون 1 2 <لصالح الكونفورمر 1 ، وهو الروتامر ذو الطاقة الأقل الذي ينتج ترددات حقيقية. تؤيد القياسات الطيفية المسجلة للأشعة تحت الحمراء والرنين النووي المغناطيسي البروتوني والكربوني-13 الكونفورمر 1 ، والذي يتم دعمه بشكل كامل من خلال المحاكاة الطيفية. تم الحصول على التحولات الكيميائية المتوقعة عند مستوى B3PW91/6-31G باستخدام طريقة الأوربتال الذرية غير المتأثرة بالمقياس (GIAO) مع وبدون استخدام نموذج الوسط المستمر القطبي .(PCM) تم اكتشاف دلائل على دوران النيتروجين الداخلي الحر والمقيد حول روابط C–N من قياسات الرنين النووي المغناطيسي. باستخدام تحليل الإحداثيات الطبيعية وتوزيعات الطاقة الكامنة ، تم اقتراح تخصيص اهتزازية كاملة ومؤكدة لجميع الأساسيات لجزيء .AMTDPC تمت إجراء دراسات مكملة حول حواجز الدوران الداخلي للحلقات CH3 و CH3S و NH2 وثياديازول . استناداً إلى قياسات الطيف التي أظهرت مستوى عالياً من التطابق مع القيم المتوقعة، يمكن استنتاج أن المطابق 1 ظهر باعتباره الأيزومر ذو أعلى استقرار. كما توجد اختلافات بسيطة بين مسافات الروابط المحسوبة وقراءات الأشعة السينية للمركبات المقارنة.

الكلمات المفتاحية: استقرار الشكل، تخصيص اهتزازي، طيف الرنين النووي المغناطيسي، تحليل الإحداثيات الطبيعية، حواجز الدوران الداخلي، وحسابات.DFT

1. Introduction

Pyrazoles are frequently employed in the pharmaceutical industry for the synthesis of biologically active derivatives [1], [2], [3].This approach has also been explored by other researchers [4], [5], [6], [7], [8].[9] , these compounds function as analgesics, anti-inflammatory agents, antibacterial agents, and antidepressants. A recent study conducted by [10] revealed that derivatives of amino-pyrazoles exhibit potential in mitigating brain-protein aggregation, a critical early step in the progression of Alzheimer's disease. There is a scarcity of information regarding the vibrational spectra and configuration of substituted pyrazoles, particularly in relation to N-substituted pyrazoles [11].[12], [13], [14].

Previous studies have examined the vibrational assignment of pyrazoles. The subject of this study, (AMTDPC, $C_7H_6N_6S_2$), exhibits several structural characteristics, such as linear -C≡N (sp), planar -NH_2 (sp2), and tetrahedral -CH_3 (sp3) moieties, in addition to the pyrazole and thiadiazol rings. As far as we know, there has been no previous investigation into the structural stability, vibrational characteristics, ^{1}H and ^{13}C NMR spectra, or obstacles to internal rotation for AMTDPC, either in theoretical or experimental studies. Furthermore, the molecular geometry and structural parameters (SPs) of AMTDPC have not been examined using any of the microwave, x-ray, electron, or neutron diffraction techniques. In the realm of vibrational spectroscopy, the significance of ab initio calculations, including Density Functional Theory (DFT) approaches and Restricted Hartree-Fock (RHF) calculations, has increased [10], [15], [16], [17], [18], [19]. In recent years, the utilization of DFT simulations using the B3PW91 method has gained recognition as a reliable approach for monitoring the molecular geometry and conformational stability of compounds of medium and large size, encompassing up to 26 atoms [20], [21], [22]. In addition, the utilization of GIAO NMR DFT-B3PW91 calculations has become prevalent in the field of interpreting chemical shifts of ^{1}H and ^{13}C [23], [24], [25], [26], [27], [28], [29], [30], [31]. Hence, this study presents a comprehensive investigation into the vibrational assignments and structural stability of AMTDPC through the utilization of infrared (IR) and nuclear magnetic resonance (NMR) spectroscopy. Additionally, theoretical predictions based on B3PW91 are incorporated, encompassing base sets up to 6-311G(d) [15], [32], [18], [19]. In order to gain insight into the intricate conformational changes inside the molecule being investigated, potential surface scans (PSS) were performed on the CH_3, CH_3S, NH_2 groups, and thiadiazol ring. Our research on barriers to internal rotations of methyl and NH2 [33], [34], [35] was enhanced by the inclusion of these investigations.

2. Experimental

The chemical substances used in this study were obtained from Aldrich Chemical Company, ensuring a minimum purity level of 98%. The materials employed in NMR and IR analysis exhibited spectroscopic characteristics. The solid sample was examined using the CsI pellet technique while IR dye was connected to a vacuum pump. The Fourier transform infrared spectrum (FT-IR) of the solid sample was recorded from 4000 to 200 cm^{-1} using a Spectrum 100 Perkin Elmer spectrophotometer equipped with Spectrum RX software. To obtain a satisfactory signal-to-noise ratio, forty scans were collected at 1.0 cm resolution with baseline correction and automatic smoothing features. In accordance with the methodology outlined by S.M. Hassan et al. [36]. The solid sample of AMTDPC was synthesized by Hassan et al. (2001) through the reaction of ketene with a hydrazine derivative. AMTDPC in DMSO-d6 was analyzed using Top Spin 1.3 software and a Bruker Avance 400 MHz spectrometer fitted with a Magnex superconducting magnet to get the 1H and 13C NMR spectra (Figures 1 and 2). The material was first dissolved in methanol and then diluted in a 50/50 (v/v) acetonitrile/water solution in a serial manner. The samples were injected into the mass spectrometer using a Harvard syringe pump (Harvard, CA, USA) at a flow rate of 10 µL per minute.

3. Results and Discussion

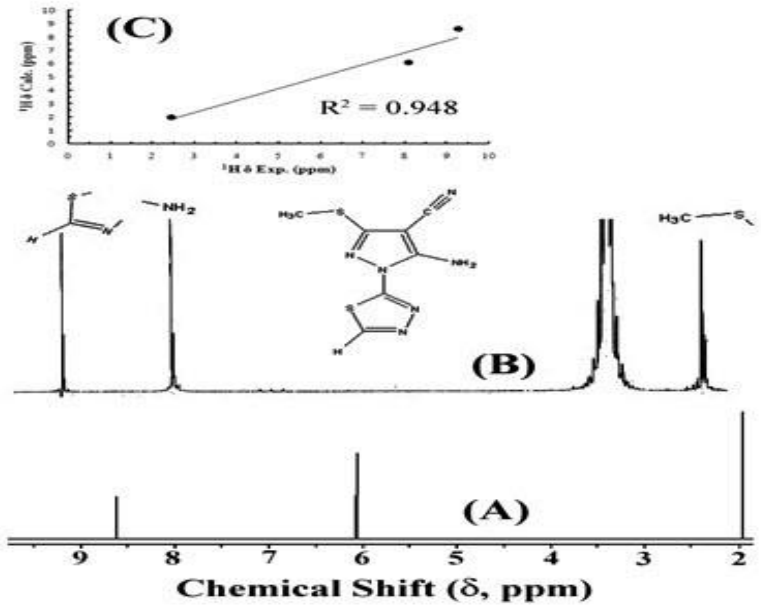

Figure 1: The ^{1}H NMR spectrum of AMTDPC, wherein the chemical shifts are recorded in parts per million (ppm). (**A**) The spectrum obtained for conformer 1 is computed using the GIAO method. (**B**) The experimental spectrum is presented, with peak assignments assigned to both spectra to highlight their differences.

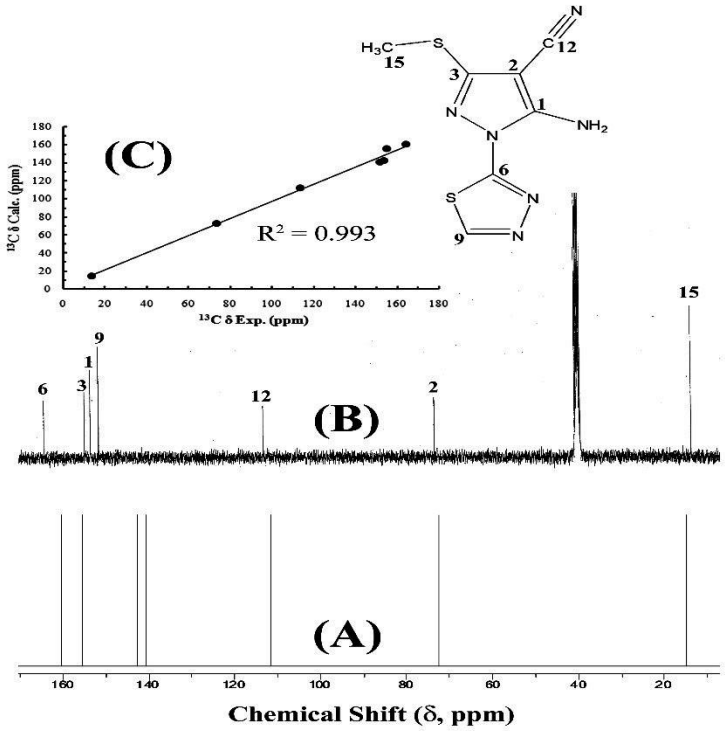

Figure 2: The ^{13}C NMR spectrum of AMTDPC, represented by chemical shifts measured in parts per million (ppm). (**A**) The spectrum obtained for conformer 1 using the GIAO method; (**B**) The experimental spectrum, with peak assignments given for both spectra to highlight their differences; (**C**) The correlation between the calculated (x-axis) and experimental peak positions.

3.1 Ab initio calculations

The Linear Combination Atomic Orbitals - Molecular Orbitals - Self Consistent Field (LCAO-MO-SCF) quantum mechanical Gaussian 09 computations were developed using the RHF and DFT methodologies [17]. Due to a lack of computer resources, frequency calculations were only conducted using B3PW91/6-31G(d) [15], [16], [18], [19], [32]

3.2 Rotational isomerism

The rotational isomerism of AMTDPC is relatively complex due to the presence of a thiadiazole ring and planar moieties CH_3, CH_3S, and NH_2 connected by single bonds. These moieties have the ability to spin and generate a total of 9 possible isomers that adhere to the Cs and C1 point group, as depicted in Figure 3. In conformer 1, the N_4 position of the pyrazole ring and the N_7 position of the thiadiazole ring are first connected in a trans configuration.

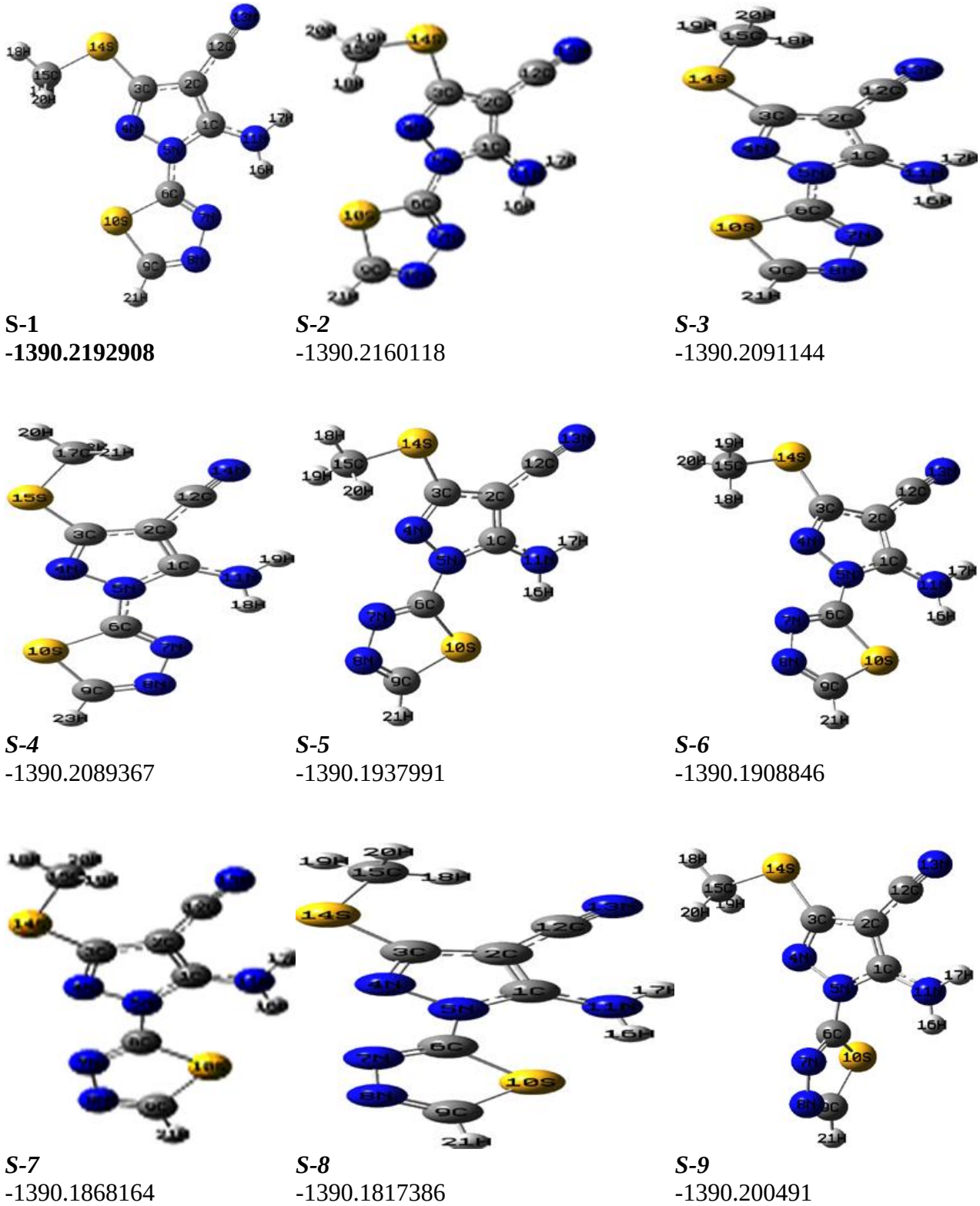

S-1
-1390.2192908

S-2
-1390.2160118

S-3
-1390.2091144

S-4
-1390.2089367

S-5
-1390.1937991

S-6
-1390.1908846

S-7
-1390.1868164

S-8
-1390.1817386

S-9
-1390.200491

Figure 3: Rotational isomerism of AMTDPC with RHF energy.

The methyl group undergoes a 180° rotation along the C_{15}–S_{14}, leading to the formation of planar NH2 groups through sp2 hybridization, resulting in Structure 2. The formation of Structure 3 involves a 180° rotation of the CH_3S moiety around the C_3−S_{14}, with CH_{18} eclipsing the bond. The formation of Structure 4 involves a second rotation of the CH_3 group by 180° around C_3−S_{14}, where CH_{18} is staggered in relation to the two lone pair electrons on sulfur. As a result, the internal rotation around the C_{15}–S_{14} and/or C_3–S_{14} bonds suggests the presence of four structures 1-4, wherein the N_7 of the thiadiazole ring and the N_4 of the pyrazole ring are in close proximity to each other. In each of these structures, the NH_2 group exhibits trigonal planar (sp2) symmetry. Structures 5-8 are formed when the N_4 and N_7 of the pyrazole and thiadiazole rings are connected in a cis configuration. Structure 9 has trigonal planar (sp2) symmetry in the NH_2 group, whereas the thiadiazole ring is oriented perpendicular to the plan.

3.3 Optimization and computational analysis of frequencies.

The gradient approach proposed by [37] is employed to concurrently facilitate the relaxation of all geometric parameters, with the ultimate goal of attaining the ideal structural parameters (SPs). The vibrational frequencies were subsequently quantified by employing computed spin perovskites (SPs) with 6-31G* basis sets, as well as the RHF and DFT-B3PW91 methodologies. The primary software utilized for doing the quantum mechanical (QM) calculations mentioned before [17], [32]was the Gaussian 09 program.

The results of the study indicated that conformer (1) displayed the minimum energy, whereas conformer (2) exhibited the maximum energy, reaching up to 1500 cm^{-1}. Notably, conformer 1, which exhibits the lowest energy structure with a trigonal planar NH2 group and trans to each other N_7 of the thiadiazole ring and N_4 of the pyrazole ring, yielded all 57 real frequencies during full optimization. This observation suggests that the AMTDPC structure is entirely planar. The expected surface areas (SPs) for conformer 1 are compared with x-ray data for substituted pyrazoles [38]to offer contextual information. Refer to Figure 3, as well as Tables 1 and 2)

TABLE (1) RHF energies in Hartrees of AMTDPC conformers **1-9**.

6-31G(d) basi set	*RHF level*	*ΔE^b (cm^{-1})*	*ΔE^b(kcal/mol)*
Structure-1	-1390.2192908	0.0	0.0
Structure-2	-1390.2160118	720	2.1
Structure-3	-1390.2091144	2234	6.4
Structure-4	-1390.2089367	2272	6.5
Structure-5	-1390.1937991	5595	16.0
Structure-6	-1390.1908846	6234	17.8
Structure-7	-1390.1868164	7127	20.4
Structure-8	-1390.1817386	8242	23.6
Structure-9	-1390.200491	4126	11.8

[a]ΔE denotes the disparity in energy between conformer 1 (minimum energy) and conformers 2-9 at the RHF level.

TABLE (2) B3PW91 and RHF structural parameters[a] for AMTDPC utilizing 6-31G(d) basis sets.

Parameters	Ref [46]	***RHF for Structure(1)***	***B3PW91for Structure(1)***
		6-31G(d)	**6-31G(d)**
r(C_1C_2)	1.379 (9)	1.383	1.397
r(C_2C_3)	1.405 (5)	1.428	1.434
r(C_3N_4)	1.305 (5)	1.288	1.317
r(N_4N_5)	1.388(5)	1.379	1.383
r(N_5C_1)	1.348 (5)	1.356	1.374
r(N_5C_6)		1.373	1.372
r(C_1N_{11})	1.358 (4)	1.331	1.340
r(C_2C_{12})	1.408 (7)	1.419	1.408
r($C_{12}N_{13}$)	1.139 (7)	1.139	1.166
r(C_3S_{14})		1.751	1.754
r($S_{14}C_{15}$)		1.810	1.814
r(C_6N_7)		1.275	1.308
r(N_7N_8)		1.365	1.362
r(N_8C_9)		1.268	1.296
r(C_9S_{10})		1.735	1.743
r($S_{10}C_6$)		1.730	1.737
r(C_9H_{21})		1.071	1.083
r($N_{11}H_{16}$)		0.997	1.008
r($N_{11}H_{17}$)		0.994	1.016
r($C_{15}H_{18}$)		1.082	1.093
r($C_{15}H_{19}$)		1.080	1.092
r($C_{15}H_{20}$)		1.080	1.092
r(N_7...H_{16})		2.158	2.058
r(N_4....H_{20})		2.803	2.775
∠($C_1C_2C_3$)		104.9	104.8
∠ ($C_2C_3N_4$)	112.2 (4)	112.0	112.4
∠ ($C_3N_4N_5$)	104.4 (3)	105.1	104.4
∠ ($N_4N_5C_1$)	111.8 (3)	112.3	112.8
∠ ($N_5C_1C_2$)	106.2 (3)	105.7	105.8
∠($N_5C_6N_7$)		123.6	123.4
∠ ($N_5C_6S_{10}$)		121.5	121.6
∠ ($C_6N_7N_8$)		112.5	112.2
∠ ($N_7N_8C_9$)		112.6	112.4
∠ ($N_8N_9S_{10}$)		115.0	115.3
∠ ($C_9S_{10}C_6$)		85.0	85.0
∠ ($N_8C_9H_{21}$)		122.8	123.0
∠ ($S_{10}C_9H_{21}$)		122.2	121.7
∠ ($C_6N_5C_1$)	129.4 (3)	128.7	127.5
∠($C_6N_5N_4$)	118.7 (3)	119.1	119.6
∠ ($C_1N_{11}H_{16}$)		120.4	119.0
∠ ($C_1N_{11}H_{17}$)		119.3	119.5

∠($H_{16}N_{11}H_{17}$)		120.3	121.5
∠ ($N_{11}C_1C_2$)	130.5 (3)	130.3	131.4
∠ ($N_{11}C_1C_5$)	123.2 (3)	124.0	123.0
∠($C_{12}C_2C_1$)	127.3 (4)	125.3	125.3
∠($C_{12}C_2C_3$)	127.4 (4)	129.8	129.9
∠($N_{13}C_{12}C_2$)	179.6 (6)	177.8	178.0
∠($C_2C_{13}S_{14}$)		124.6	124.4
∠($S_{14}C_3N_4$)		123.4	123.1
∠($C_3S_{14}C_{15}$)		100.8	100.1
∠($H_{18}C_{15}S_{14}$)		105.9	105.9
∠(H_{19} $C_{15}S_{14}$)		110.8	110.8
∠(H_{20} $C_{15}S_{14}$)		110.8	110.8
∠($H_{18}C_{15}H_{19}$)		109.7	109.8
∠($H_{18}C_{15}H_{20}$)		109.7	109.8
∠($H_{19}C_{15}H_{20}$)		109.9	109.7
τ$C_3S_{10}C_{11}H_{22}$		61.1	61.0
A, MHz		817	814
B, MHz		343	339
C, MHz		242	240
μ_{tot}, Debye		5.574	5.173

[a] Bond distances are expressed in angstroms (Å), while bond and dihedral angles are denoted in degrees. Rotational constants A, B, and C are measured in megahertz (MHz), and the total dipole moment (μ_{tot}) is quantified in Debye

3.5 Structural parameters

The C-N distances for C_1-N_{11} and C_6-N_5 are approximately 0.03-0.09 P shorter than those reported for AP (1.429 P), ATP (1.370 P), and adenine (1.357 Å) (Mohamed et al., 2008, 2009; Soliman et al., 2007). The calculated SPs (refer to Table 2) for AMTDPC highlight the double-bond nature of these bonds (see atom numbering in Figure 7). Furthermore, it is anticipated that the distances between C_6-N_5 and C_1-N_5 will be shorter than those between C_1-N_{11} by approximately 0.043 Å, suggesting a greater level of double-bond nature for C_6-N_5 and C_1-N_5 in comparison to C_1-N_{11}. The aforementioned projection is consistent with the calculated rotational barriers of NH2, the detection of distinct N-H bonds based on NMR findings, and the observed stretching bands of NH_2. The following sections will explore these findings in greater detail.

In contrast to 2-aminophenol (2AP) and 2-aminothiophenol (2ATP), the SPs for AMTDPC exhibit a preference for trigonal planar (sp2; NH_2) NH_2 groups rather than trigonal pyramidal (sp3; NH_2) NH_2 groups. It is worth mentioning that the angles of $N_5C_1C_2$ and $C_{12}C_2C_1$ are estimated to fall within a range of 0.4-2.5 Å when compared to the values derived from x-ray crystallographic data [38], [39], [40]. On the other hand, there are small differences (0.01-0.04 Å) between the calculated bond distances and the x-ray readings. The x-ray crystallographic data of 3-amino-4,5-dicyano-1-methylpyrazole [38]

and 5-amino-4-cyano-1-phenylpyrazole (Zukerman-Schpector et al., 1994) reveal variations in bond lengths and bond angles, with values ranging from 0.3-5.0% and 2.0-4.0%, respectively.

The N….H bond lengths for AMTDPC have been calculated to range from 2.06 to 2.80 Å, with the combined Van der Waal radii of the hydrogen and nitrogen atoms being 2.75 Å [41], [42]. Therefore, in addition to the anticipated intermolecular hydrogen interactions in AMTDPC, it is expected that there would be moderate intramolecular hydrogen bonding interactions between N7...H16 and N4...H20, as seen in Table 2.

3.6. Simulated infrared Spectra

The projected intertwining of the predicted infrared (IR) normal modes is expected to exhibit a reasonably high amount of interaction, particularly for bigger molecules. As a result, the utilization of projected infrared spectra has been proposed by [20], [43] as a valuable method for conducting vibrational studies on organic molecules. Simulated vibrational spectra can be generated by utilizing both infrared (IR) intensities and Raman activity, along with their polarizability and dipole moment derivatives.

The frequencies and infrared intensities of the single conformer (1) were simulated using the B3PW91 density functional theory (DFT) approach, in conjunction with a 6-31G(d) basis set. The IR spectrum seen in Figure 4 was constructed using the dipole moment derivatives, as described in the entire technique outlined in Reference [44]. The agreement between the estimated and observed frequencies, as shown in Table 3, provides strong support for the vibrational assignments. Nevertheless, the calculated infrared (IR) intensities denoted as w, m, and s below 1000 cm^{-1} do not correspond with the solid's IR spectrum, which exhibits strong to extremely strong intensities.

In spite of the significant spectral overlap observed in the recorded infrared (IR) spectrum, it is worth mentioning that the projected IR intensities exhibited superior performance compared to the anticipated Raman activity inside the CH stretching region.

3.7 Simulated NMR spectra

Previous studies have shown that chemical shifts (, ppm) for small isolated molecules can be accurately predicted using DFT NMR calculations with the Gauge-invariant atomic orbitals (GIAO) model [15], [24], [29], [30], [31]. In recent years, there has been an increase in the popularity of these calculations [27]. The preference for DFT predictions over the RHF technique has been shown in certain studies [30], [45]. However, it is crucial to note that the accuracy of NMR theoretical predictions is primarily influenced by two key factors: the optimized structural parameters and the implemented basis set. The simulated spectra were computed using the B3LYP/6-31G(d) structural parameters for conformer 1 in this particular instance. Chemical shifts were predicted at the B3LYP/6-311+G(2d,p) level using the Gauge-invariant atomic orbitals (GIAO) method, as described by Chesnut and Phung in 1989. These predictions were then compared to the calculated chemical shifts obtained through the use of the same technology, namely TMS. The GIAO calculations were conducted using the Polarizable Continuum Model (PCM) implicit salvation approach[46], [47], considering both the solvent's impact and not. The NMR prediction also incorporated the solvent. The results presented in Figures 1 and 2 pertain to individuals who employed the phase change material (PCM) due to its observed ability to improve the concordance between experimental and calculated outcomes.

4. Vibrational assignments

In the infrared and Raman spectra of AMTDPC, fifty-seven fundamentals are anticipated, and all of them are Raman and IR active. In addition to the $\nu_{C\equiv N}$ stretch around 2300 cm1, sex vibrations were anticipated in the high frequency region 2900-3500 cm^{-1} ($\nu_{1\text{-}5}$ and ν_{39})). Below 200 cm^{-1}, which is beyond the range of our instrumental detection capabilities, nine fundamentals are expected. As a result, 41 bands between 1700 and 200 cm1 had to be assigned. Vibrational assignments were compounded by the vast number of basics and occasionally the substantial mixing. The infrared frequencies presented in the subsequent sections are extracted from the solid sample's spectrum within a CsI matrix, as seen in Table 3.

4.1 NH_2 Fundamentals vibrations.

Hydrogen bonding interactions do not appear to significantly alter or affect the N-H stretching fundamentals. The recorded infrared spectrum exhibits distinct and well-defined bands, consistent with the estimated infrared intensity (Figure 4). The infrared (IR) bands seen at 3376 and 3295 cm-1 (vs) were confirmed to correspond to two distinct stretching modes of NH2, namely ν1 and ν2. The measured stretching modes of NH are shifted towards lower frequencies by approximately 200 cm as a result of inter- and intramolecular hydrogen bonding. Furthermore, the empirical relationship of $\nu_s = 345.5 + 0.876\,\nu_{as}$ [48], where s and as are in wavenumbers, is not followed by the ν_s and ν_{as} NH_2 stretches. This finding implies that the amino groups' N–H bonds are not interchangeable.

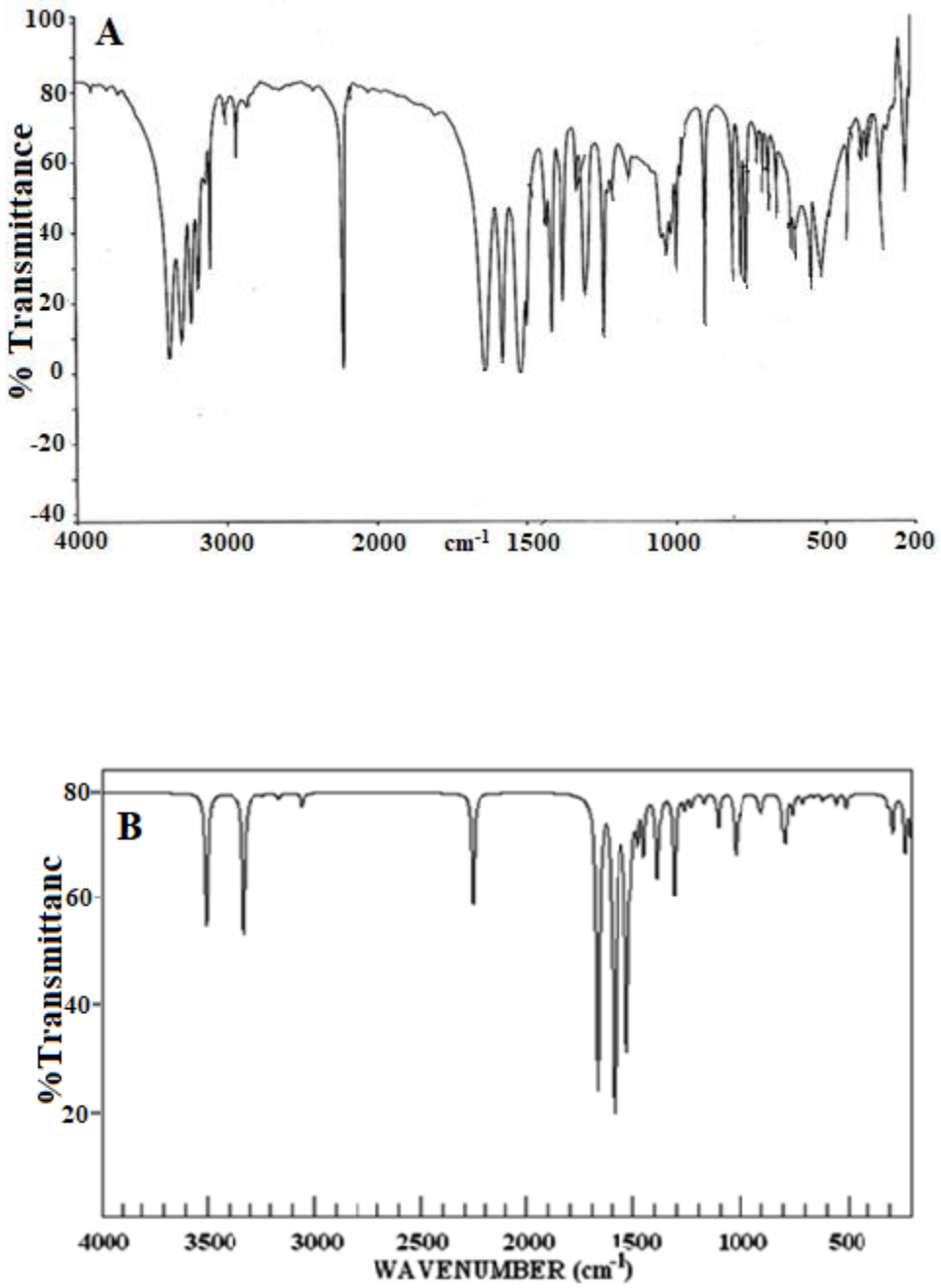

Figure 4: Experimental (A) and Calculated (B) Infrared spectrum of AMTDPC.

Table 3: B3PW91/6-31G(d) calculated and observed frequencies for AMTDPC.

Species	Calculated				Observed	Assignment
	Unscaled	Scaled	IR Int.	Raman act.	IR	
A′	3717	3508	126.6	54.4	3376 vs	ν_{as} NH_2
A′	3526	3330	136.7	100.2	3295 vs	ν_{s} NH_2
A′	3277	3240	1.5	192.9	3231 s	νC_9H_{21} (Thiadiazole ring)

A′	3190	3165	2.8	96.2	3184s	ν_{as} CH_3
A′	3088	3055	10.9	128.0	3105 w	ν_{s} CH_3
A′	2342	2260	102.9	385.6	2218 vs	νC≡N
A′	1703	1675	417.7	9.1	1637 s	$\delta_{scissor}$ NH_2
A′	1625	1590	487.1	102.6	1577 s	νCC (Pyrazole ring)
A′	1573	1530	306.0	435.7	1517s	νN_5C_6 (bridge)
A′	1557	1510	40.2	18.1	1496m	νCN (Pyrazole ring)
A′	1507	1498	5.8	32.4	1490 sh	νCN (Thiadiazole ring)
A′	1499	1480	30.8	5.2	1472 w	δ_{as} CH_3
A′	1471	1452	36.1	95.8	1412 s	νCN (Pyrazole ring)
A′	1421	1390	70.4	15.0	1388 wsh	δ_{s} CH_3 (Umbrella mode)
A′	1384	1370	11.0	15.1	1375 s	νC—N
A′	1336	1310	90.3	41.9	1329 w	νCC (Pyrazole ring)
A′	1280	1265	12.1	72.8	1301m	δ_{ip} C_9H_{21} (Thiadiazole ring)
A′	1249	1233	11.1	16.0	1238 s	νC_2C_{12} (exocyclic C−C)
A′	1207	1175	7.1	31.5	1152 w	νN−N (Pyrazole ring)
A′	1111	1111	28.1	5.8	1081 w	νN−N (Thiadiazole ring)
A′	1054	1025	14.8	0.3	1046 wsh	ρ NH_2
A′	1032	1019	41.3	8.3	1028 wsh	νC_3S_{14} (exocyclic C−S)
A′	1012	1000	8.4	8.1	1013 wsh	δ_{as} CH_3
A′	912	900	15.3	22.8	900 vs	δ_{ip} NNC (Thiadiazole ring)
A′	799	788	36.4	26.3	779 m	Ring breathing (Pyrazole ring)
A′	765	755	16.0	4.3	763 m	νC−S (Thiadiazole ring)
A′	733	720	0.9	7.4	722 w	ν S_{14}−C_{15} (S−CH_3)
A′	697	688	2.4	2.8	686 w	Ring breathing (Thiadiazole ring)
A′	672	660	2.6	8.3	659 w	δ_{ip} C_2C_{12} (exocyclic C−C)
A′	617	600	2.9	13.9	598 w	δ_{ip} CSC (Thiadiazole ring)
A′	483	477	1.8	2.0	482 wsh	δ_{ip} C−C≡N
A′	424	420	0.7	2.8	419 w	δ_{ip} (Pyrazole ring)
A′	361	355	0.4	1.6	357 w	δ_{ip} N_5C_6 (bridge)
A′	306	305	7.7	6.1	312 m	δ_{ip} C_3 −S_{14}−C_{15} (C−S−CH_3)
A′	287	287	9.5	1.3	264 w	δ_{ip} C_1− N_{11} (C−NH_2)
A′	196	196	18.2	2.4	211 wsh	δ_{ip} $N_5C_6S_{10}$ + δ_{ip} $N_4C_3S_{14}$
A′	100	100	1.5	5.9	—	δ_{ip} C≡N
A′	95	95	2.9	0.8	—	δ_{ip} (Pyrazole ring)
A″	3189	3159	2.5	36.0	3120 w	ν_{as} CH_3
A″	1483	1450	11.4	22.1	1430 w	δ_{as} CH_3
A″	998	998	5.2	4.7	995 m	ρ CH_3
A″	801	801	21.6	1.7	807 m	δ_{wag} C_9H_{21}(Thiadiazole ring)
A″	723	710	6.8	1.1	705 w	Pyrazole ring Torsion
A″	639	619	5.3	0.4	616 vw	Pyrazole ring Torsion
A″	625	910	5.6	0.3	611 wsh	Thiadiazole ring Torsion
A″	577	557	8.7	0.6	544 m	δ_{twist} NH_2
A″	549	519	0.1	0.3	(509 wbr)	Thiadiazole ring Torsion
A″	528	511	12.7	5.5	(509 wbr)	$\delta_{wag.}$ C_2C_{12} (exocyclic C−C)
A″	376	376	0.2	0.1	373 w	Pyrazole ring Torsion
A″	281	281	25.8	0.7	289 w	Ring Torsion
A″	225	225	44.7	2.5	227 m	Ring Torsion (Butter fly)
A″	182	182	163.5	0.02	—	δ_{wagg} NH_2
A″	154	154	2.0	0.4	—	CH_3 Torsion
A″	114	114	0.5	0.4	—	NH_2 Torsion
A″	61	61	0.1	0.04	—	δ_{wagg} S_{14}−C_{15} (S−CH_3)
A″	45	45	0.1	0.4	—	Ring Torsion
A″	35	35	8.5	0.5	—	Ring Torsion

Based on the findings of Jesson

(1958), Soliman et al. (2007), Mohamed et al. (2008), and Mohamed et al. (2009), it has been observed that the NH2 scissoring frequency falls within the spectral range of 1950-1650 cm^{-1}. According to Table 3, there are two predicted bending modes of A′ NH2 at 1703 ($\nu 7$) and 1054 ($\nu 21$) cm^{-1}. Therefore, the unscaled NH_2 scissor mode, κ7 at 1703 cm-1, aligns with the previously documented highly intense infrared bands observed at 1637 cm^{-1} [34], [35], [49]. On the other hand, the NH2 rock ($\nu 21$) is associated with the faint infrared band detected at 1046 cm^{-1} (predicted at 1054 cm^{-1}).

4.2 CH and CH_3 fundamental vibrations

The C9-H21 stretching of the thiadiazole ring is associated with the conspicuous infrared band observed at 3231($\nu 3$), which is calculated to be 3240 cm^{-1}. In addition, the C-H bending mode ($\nu 17$), which is calculated at a wavenumber of 1280 cm^{-1}, is associated with the medium-infrared band found at 1301.

The week band at 3105 cm1 fit the A′ stretch species (ν_5), while the two methyl C- stretches (A′ and A″) are attributed to the detected IR bands at 3184 (ν_4) and 3120 (ν_{39}) cm^{-1}, respectively. Between 980 and 1500 cm^{-1} there are predicted to be five vibrational modes (CH_3 bending and rocking) (3A′; ν_{12}, ν_{14} and ν_{23} and 2A″; ν_{40} and ν_{41}). As a result, the IR bands that are detected at 1472 and 1430 $cm^{-1}$are attributed to ν_{12} and ν_{40}, which are 42 cm^{-1} apart (estimated at 1499 and 1483 cm^{-1}), respectively.

Furthermore, the measured shoulders at 1388 cm^{-1} in the IR spectrum are consistent with the umbrella modes (ν_{14}). While the second methyl rock (ν_{23}) was attributed to the measured IR band at 1013 cm1 reported earlier at 1013 cm1, the first methyl rock (ρCH_3;υ_{41}) is predicted/seen at 998/995 cm^{-1} in the IR spectra [49]. It was attributed to the faint Calc IR at 154 cm^{-1}due to the methyl torsion mode's extremely low IR intensity (ν_{53}). However, due to the Rayleigh scattering background below 100 cm^{-1}, the CH_3S torsion (ν_{55}) was not visible (Figure 4).

4.3 Heavy atom stretching fundamentals

The C≡N bond (υ6) exhibited a direct correlation with the highly intense infrared band seen at 2218 cm^{-1}. The C=C stretch (υ8) is observed at a wavenumber of 1577 (s, IR) cm^{-1}, which aligns well with the calculated infrared intensity of 487.1 kcal/mol. The presence of a prominent infrared band at 1517 cm^{-1} can be ascribed to the C≡N (υ9) group of the pyrazole ring, as evidenced by the substantial intermixing of the three C≡N stretching vibrations (υ9, υ10, and υ11). This corresponds to the infrared intensity band at 1573 cm^{-1}, which has been determined to be high.

In addition, the calculated infrared intensities of the three C≡N stretching modes (υ13, υ15, and υ24) exhibit a rather moderate level of intensity, which contradicts the observed bands. These modes can be considered as being inherently mixed. These C were allocated to the identified infrared bands at 1412 (s), 1375 (s), and 900 (vs) cm^{-1}.

The C_2–C_3 (υ16) and C_2–C_{12} (υ18) segments in the infrared spectrum were predicted to have high and low intensities, respectively. The infrared bands at 1329/1336 and 1238/1249 cm^{-1} were assigned to (υ16) and (υ18) respectively, within the spectral range of N-methylpyrazole, as determined by Orza et al. (1997). Moreover, it is expected that υ_{N-N} (υ19 and υ20) will either be prohibited or significantly diminished in the infrared spectrum. Consequently, when comparing the medium band observed at 1056 cm^{-1} with the weak infrared (IR) bands discovered at 1152 and 1081 cm^{-1}, respectively, it is possible that these bands correspond to the υ_{N-N} stretches, as suggested by Durig et al. (1992).

The AMTDPC molecule consists of two rings, namely pyrazole and thiadiazole. These rings enable the observation of the A' ring bending modes (υ28 and υ30) in the infrared (IR) spectra at approximately 686 and 598 cm^{-1}, respectively. In contrast, the IR spectra at 419(w) cm^{-1} and out of ray light revealed the other two ring bending modes (υ32 and υ38), respectively.

Due to the expected occurrence of the out-of-plane ring bending modes (υ56 and υ57) below 100 cm 1, they cannot be observed experimentally. According to the computed frequencies, the C_6S_{10} (25 cm^{-1}) and C_9S_{10} (26 cm^{-1}) segments were found to be separated by 34 cm^{-1}. This separation aligns with the observed infrared bands at 779 cm^{-1} and 763 cm^{-1}, respectively. Similarly, the infrared (IR) bands detected at 1028/1032 cm^{-1} and 722/733 cm^{-1} were assigned to the C_3S_{14} (υ22) and $C_{15}S_{14}$ (υ27)) strains, respectively. The δ_{ip} C–S (υ35) could potentially be linked to CCS bending, as evidenced by the presence of a poorly resolved week at 312 cm^{-1} (estimated at 306 cm^{-1}) in the infrared spectra.

5. NMR spectral interpretations

The simulated and experimental ^1H and ^{13}C NMR spectra showed a remarkably high level of agreement, as shown in Figures 1 and 2. This confirms the established structural properties of AMTDPC's conformer 1. According to the prediction made by Chesnut and Phung in 1989, the signal observed at 1.96 ppm is attributed to three protons belonging to the CH_3 group, which are located at 2.44 ppm. This is achieved by calculating the average chemical shifts of similar hydrogen atoms. The GIAO prediction also yields positive signals for NH_2 protons. The measured spectrum has a wide singlet peak at 8.09 ppm, which corresponds to two protons of the NH_2 group. These protons are estimated to be located at 6.06 ppm. The singlet observed at 9.26 ppm can be attributed to the CH proton of the thiadiazole ring, which was determined to be 8.61 ppm.

6. Barriers to internal rotation.

Figure 1C demonstrates a robust correlation between the theoretical and experimental chemical changes, as evidenced by the high R2 value of 0.948. Moreover, the correlation between the theoretical and experimental chemical shifts resulting from the 13C NMR GIAO prediction is clearly demonstrated in Figure 2C, where R2 is equivalent to 0.993 (Chesnut and Phung 1989). The signals seen at 164.43, 155.09, 153.72, and 151.8 ppm were assigned to the carbons C6, C3, C1, and C9, respectively, as indicated in Tables 4, 5, and Figure 2. Furthermore, the observed signals at 113.64, 73.72, and 13.70 ppm were ascribed to the remaining three carbon atoms, namely C12, C2, and C15. The obtained results exhibit a high level of concurrence with the computed values depicted in Figure 2. The restricted photosystem simulations (PSS) were performed using the optimized spin perovskites (SPs) of conformer 1, which were computed at the B3LYP/6-31G(d) level. The critical structure for internal rotations around C is believed to be Conformer 1, which is considered the global minimum for internal rotations around CS, CN, and CC single bonds. After rotating the CH_3, CH_3S, NH_2 groups, and thiadiazole ring, conformer 1's symmetry shifts from Cs to C1, where the methyl hydrogens are no longer equal. As a result, neither the NH_2 moiety nor the methyl group are longer C_2V symmetry rotors.

Table 4 Theoretical and experimental ^{1}H NMR chemical shift values expressed in parts per million (ppm) for AMTDPC.

	Chem draw	DFT, B3PW91/6-311G(d)		Experimental (DMSO-d_6)
		Without solvent	With solvent (DMSO-d_6)	
H_{16}	6.51	5.36	6.06	8.09
H_{17}	6.51	5.36	6.06	8.09
H_{18}	2.53	1.7	1.96	2.44
H_{19}	2.53	1.7	1.96	2.44
H_{20}	2.53	1.7	1.96	2.44
H_{21}	9.00	7.56	8.61	9.26

Table 5 Theoretical and experimental ^{13}C NMR chemical shift values expressed in parts per million (ppm) for AMTDPC.

	Chem draw	DFT, B3PW91/6-311G(d)		Experimental ($CDCl_3$)
		Without solvent	With solvent ($CDCl_3$)	
C_1	159.0	139.75	142.6	153.72
C_2	92	70.28	72.47	73.72
C_3	132	151.14	155.43	155.09
C_6	162.7	156.84	160.42	164.43
C_9	152.1	137.99	140.79	151.80
C_{12}	117.0	98.51	111.81	113.64
C_{15}	12.8	13.45	14.76	13.70

6.1 CH_3 Barriers to internal rotation

Conformer 1 from Table 2 SPs was used to create the PSS curve shown in Figure 5, as stated earlier. When the dihedral angle ($H_{18}C_{15}S_{14}C_3$) is rotated in 10˚ increments, the estimated energy of conformer 1 in B3LYP/6-31G(d) increases until it reaches its maximum value at 60-70˚ (2). The energy barrier for conformer 1 is 643 cm^{-1}. The emergence of Structure 1' occurs at around 120-130 degrees as the dihedral angle undergoes further rotation. The structure of 1' (C1) closely matches that of 1 (Cs), with the exception of the non-equivalence of the out-of-plane hydrogens (H_{18} and H_{19}). A 356 cm^{-1} barrier is located between 1' and 2. Following the complete optimization of structure 2 and structure 1, calculations were performed to determine the energies and harmonic vibrational frequencies. In both instances, the presence of an imaginary frequency signifies the occurrence of transitional periods for the two structures.

The calculated values of 689 cm^{-1} for trimethyldisilane[50], as well as the average values of 703 cm^{-1} for trans,trans-2,4-hexadiene[51], 448 cm^{-1} for 1,1,1-trifluoro-propane-2-thione[52], and 392 cm^{-1} for 1,1,1-trifluoroacetone [49], seem to be in line with the estimated methyl barriers of 643 and 356 cm^{-1} for AMTDPC. According to Mohamed and Abo Aly (2004), the theoretical values of 493±21 cm^{-1}, obtained from the far infrared spectrum of trans,trans-2,4-hexadiene, exhibit a strong correlation with the experimental results of 727±3.5 cm^{-1} (FIR) for propene[53] and 773 cm^{-1} for isobutene[54]. Therefore, the values of the methyl barrier to internal rotation, as reported by Durig and Church (1980), Durig et al. (1989, 1977), Mohamed (2003), Mohamed and Abo Aly (2004), and Mohamed and Farag (2005), exhibit a strong concurrence between theoretical and experimental data.

6.2 CH_3S barriers to internal rotation

In accordance with conformer 1, the CH_3S group exhibited rotational movements around the C-S bond in increments of 10, akin to the methyl moiety. The CH_3 group is orientated towards the C-N moiety at ($N_4C_3S_{10}C_{11}$) approximately 130º, resulting in a local minimum at C1. This occurs after a peak in energy, where the CH_3 moiety is nearly perpendicular to the pyrazole ring (C1 symmetry). The energy of the CH_3 component rises as it reaches C N at around 180º. According to the information shown in Figure 6, the CH_3S barriers are seen to be 1170, 1330, and 3874 cm^{-1}, indicating a preference for conformer 1 at a dihedral angle of zero degrees.

After conducting comprehensive geometry relaxation and frequency calculations, it has been ascertained that the C1 conformer exhibits an imaginary frequency transition state at a position of 130 degrees. Based on the results obtained, it can be concluded that conformer 1 is the only AMTDPC conformer. Although there is no existing literature on experimental CH_3S rotation barriers, it is clear that the CH_3S barriers calculated in this study are 1.5–2 times higher than the previously described CH_3 barrier. This proposition is deemed rational given the comparative dimensions of the carbon and sulfur atoms.

It is important to mention that the expected CH_3 barriers for ethylsilane[22], [55] and chloroethylsilane[44] were found to be between 1071 and 1483 cm^{-1}, which aligns closely with the experimental results of 1348 cm^{-1} (far infrared) and 918±3.6 cm^{-1} (MW), respectively.

6.3 Planar NH_2 barriers to internal rotation

Figure 7 illustrates the impact of NH_2 groups on internal rotation. When the NH_2 groups are perpendicular to the plane of AMTDPC, they exhibit extreme positions. Conversely, when the NH_2 groups are positioned at shallow angles to the ring, there are less energy structures. The calculated rotational barriers for NH_2 are 6251 cm^{-1}. According to Badawi (2005) and Van Dyck et al. (2018), it is important to highlight that the NH_2 barriers for CH_2=CH–NH_2, O=C=CH–NH_2, and CH_3–CH_2–NH_2 often fall within the range of 1.0–3.3 kcal/mole (350-1154 cm^{-1}). The calculated obstacles are deemed excessively substantial to justify additional scrutiny of these formations. Nevertheless, it is important to recognize that the existing NH_2 barriers are merely approximations due to the absence of a comprehensive optimization at the maximum sites. However, according to the NMR observations and computational findings, it is evident that the NH_2 barriers are significant, even when taking into account the double bond (π) nature of the NH_2 group.

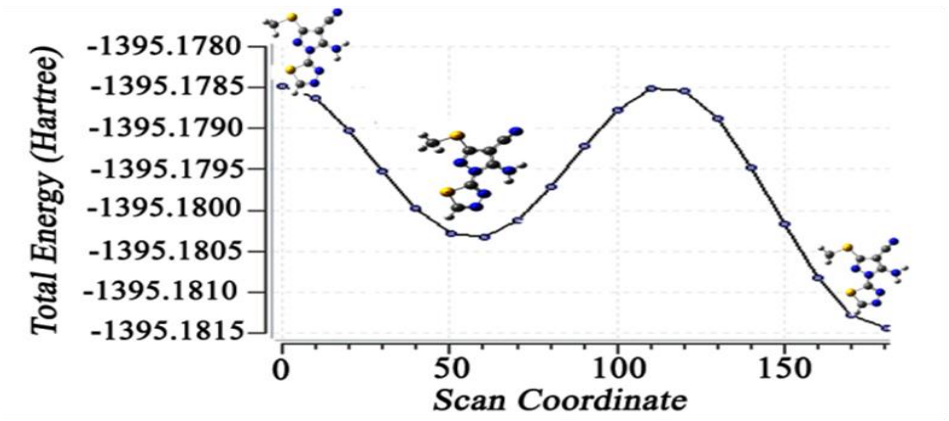

Figure 5: The barriers to internal rotation of the CH_3 group in AMTDPC, obtained through a potential surface scan using the B3PW91/6-31G(d) method.

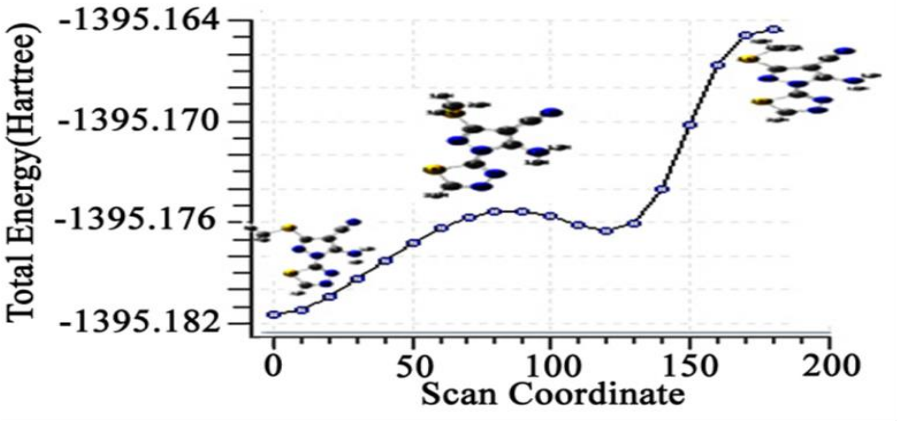

Figure 6: The barriers to internal rotation of the CH_3S group in AMTDPC, obtained through a potential surface scan using the B3PW91/6-31G(d) method.

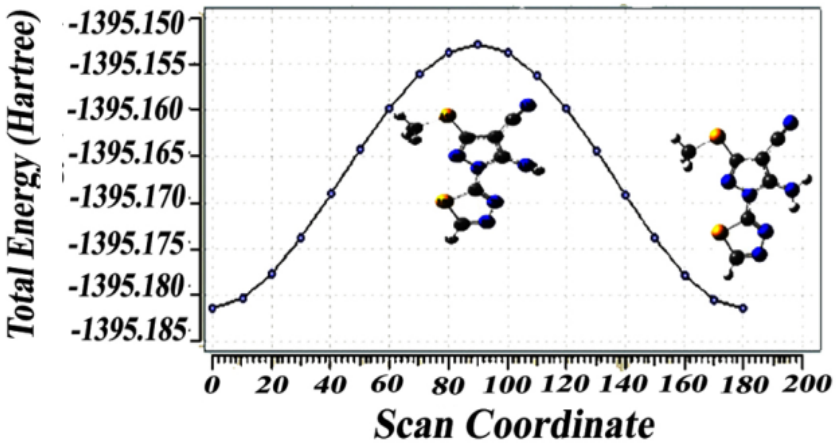

Figure 7: The barriers to internal rotation of the NH_2 group in AMTDPC, obtained through a potential surface scan using the B3PW91/6-31G(d) method.

6.4 Thiadiazole ring barriers to internal rotation

A stiff potential surface scan (PSS) was conducted using the optimized SPs obtained from B3PW91/6-31G(d) methods in order to examine the possible presence of a non-planar arrangement of the thiadiazole ring. The present study focused on the manipulation of the dihedral angle τ ($N_4N_5C_6S_{10}$), which is known to have a significant role in the structural interconversions.

As depicted in Figure 8, the thiadiazole ring exhibits maximum at a perpendicular orientation to the AMTDPC plane, namely at 4958 cm^{-1}, and a lower energy structure at 4945 cm^{-1} when the angular separation ($N_4N_5C_6S_{10}$) is around 130°. Subsequently, as depicted in Figure 8, the energy exhibits a steady rise until it reaches its peak magnitude, culminating in structure 5 and an energy barrier of 7634 cm^{-1}.

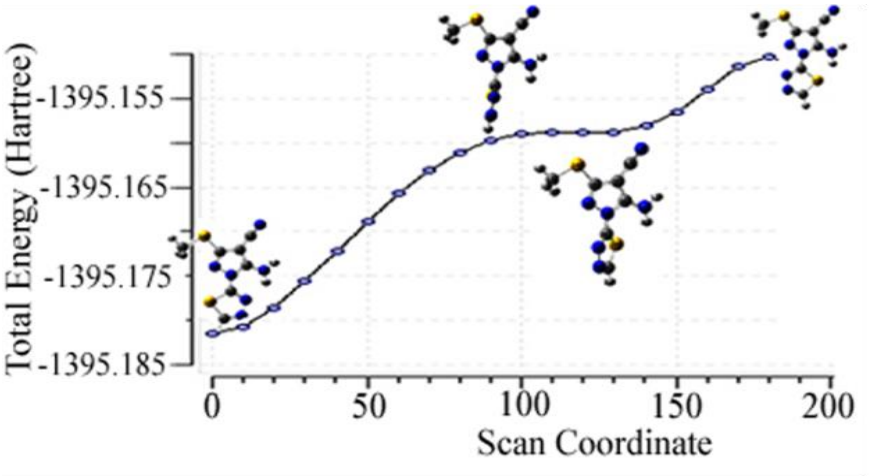

Figure 8: Barriers to internal rotations within the rings of AMTDPC, derived from a potential surface scan utilizing the B3PW91/6-31G(d) method.

7. Conclusion

The compound (AMTDPC, $C_7H_6N_6S_2$) has undergone extensive spectroscopic investigation, resulting in significant findings about its dynamic characteristics and structural attributes. The utilization of ^{1}H and ^{13}C nuclear magnetic resonance (NMR) spectra, along with infrared spectra within the 4000–200 cm^{-1} range, has played a pivotal role in elucidating the molecular intricacies of AMTDPC. The research of rotational isomerisms induced by internal rotation around C–N and/or C–S bonds led to the identification of nine isomers. Quantum mechanical simulations employing the RHF and DFT/B3PW91 techniques enhanced our comprehension, ultimately uncovering two conformers (1-2) with energies below 1000 cm^{-1}. Based on spectrum measurements that exhibited a high level of concurrence with the anticipated values, it may be concluded that conformer 1 emerged as the isomer with the highest stability. Furthermore, the chemical shifts predicted using the GIAO approach, both with and without solvent inclusion (PCM), provided confirmation for our spectroscopic findings. By comparing our results with those of related chemicals, we were able to provide more support and context to our conclusions. Our NMR findings provided clarification on the dynamic nature of AMTDPC, revealing evidence of both restricted and free NH_2 internal rotation around C-N bonds. A reliable vibrational assignment was achieved for all observable fundamentals by the utilization of potential energy distributions and study of normal coordinates. The extensive investigation on the torsional barriers to internal rotation of CH_3, CH_3S, NH_2, and the thiadiazole ring has significantly improved our understanding. This research has provided crucial insights into the dynamic behavior of AMTDPC. The combination of experimental data and quantum mechanical simulations has for a comprehensive examination of the molecular structure, conformational dynamics, and vibrational properties of AMTDPC. The aforementioned finding serves as a fundamental basis for subsequent inquiries in the domains of molecular spectroscopy and structural analysis, thereby enhancing our comprehension of associated compounds.

References

[1] M. H. Baren, S. A. Ibrahim, M. M. Al-Rooqi, S. A. Ahmed, M. M. El-Gamil, and H. A. Hekal, "A new class of anticancer activity with computational studies for a novel bioactive aminophosphonates based on pyrazole moiety," *Scientific Reports*, vol. 13, no. 1, p. 14680, 2023.

[2] P. Mahesh *et al.*, "Antiproliferative Activity of New Pyrazole-4-sulfonamide Derivatives: Synthesis and Biological Evaluation," *ACS Omega*, vol. 8, no. 29, pp. 25698–25709, Jul. 2023, doi: 10.1021/acsomega.2c07539.

[3] M. Mantzanidou, E. Pontiki, and D. Hadjipavlou-Litina, "Pyrazoles and pyrazolines as anti-inflammatory agents," *Molecules*, vol. 26, no. 11, p. 3439, 2021.

[4] K. R. Jyothikumari, K. N. Rajasekharan, and K. Dhevendran, "Synthesis of Some New Pyrazolo3', 4-d-pyrimidine Derivatives and their Antibacterial Activity," *Journal of the Indian Chemical Society*, vol. 68, no. 10, pp. 578–580, 1991.

[5] T. A. Mohamed, A. M. Hassan, U. A. Soliman, W. M. Zoghaib, J. Husband, and M. M. Abdelall, "Infrared, Raman and NMR spectra, conformational stability, normal coordinate analysis and B3LYP calculations of 5-amino-4-cyano-3-(methylthio)-1H-pyrazole-1-carbothioamide," *Journal of molecular structure*, vol. 985, no. 2–3, pp. 277–291, 2011.

[6] T. A. Mohamed, A. M. Hassan, U. A. Soliman, W. M. Zoghaib, J. Husband, and M. M. Abdelall, "Infrared, Raman and NMR spectra, conformational stability, normal coordinate analysis and B3LYP calculations of 5-amino-4-cyano-3-(methylthio)-1H-pyrazole-1-carbothioamide," *Journal of molecular structure*, vol. 985, no. 2–3, pp. 277–291, 2011.

[7] V. J. Ram, U. K. Singha, and P. Y. Guru, "Chemotherapeutic agents XI: synthesis of pyrimidines and azolopyrimidines as leishmanicides.," *European Journal of Medicinal Chemistry*, vol. 25, no. 6, pp. 533–538, 1990.

[8] R. K. Robins, "Potential Purine Antagonists. I. Synthesis of Some 4,6-Substituted Pyrazolo [3,4-d] pyrimidines [1]," *J. Am. Chem. Soc.*, vol. 78, no. 4, pp. 784–790, Feb. 1956, doi: 10.1021/ja01585a023.

[9] A.-R. Farghaly, S. A. Ahmed, K. S. Ismail, D. Ibrahim, N. Amri, and S. Elgogary, "Synthesis, antitumor activity, antimicrobial evaluation and molecular docking studies of some hydrazone, 1, 3, 4-oxadiazole, 1, 2, 4-triazole and pyrazole derivatives bearing nicotinoyl moiety," *Results in Chemistry*, vol. 7, p. 101474, 2024.

[10] P. Rzepecki, M. Wehner, O. Molt, R. Zadmard, K. Harms, and T. Schrader, "Aminopyrazole Oligomers for β-SheetStabilization of Peptides," *Synthesis*, no. 12, pp. 1815–1826, 2003, doi: 10.1055/s-2003-41031.

[11] O. Ebenezer, M. Shapi, and J. A. Tuszynski, "A review of the recent development in the synthesis and biological evaluations of pyrazole derivatives," *Biomedicines*, vol. 10, no. 5, p. 1124, 2022.

[12] W. Abisha, D. A. Dhas, S. Balachandran, and I. H. Joe, "Synthesis, Structural, and Quantum Chemical Spectroscopic, Hydrogen Bonding, and Molecular Docking Investigation of Antifungal Compound Pyrazole-Pyrazolium Picrate," *Polycyclic Aromatic Compounds*, vol. 43, no. 9, pp. 8455–8481, Oct. 2023, doi: 10.1080/10406638.2022.2149571.

[13] K. Karrouchi *et al.*, "Synthesis, X-ray structure, vibrational spectroscopy, DFT, biological evaluation and molecular docking studies of (E)-N'-(4-(dimethylamino) benzylidene)-5-methyl-1H-pyrazole-3-carbohydrazide," *Journal of Molecular Structure*, vol. 1219, p. 128541, 2020.

[14] P. Rejnhardt and M. Daszkiewicz, "Crystal structure and vibrational spectra of salts of 1H-pyrazole-1-carboxamidine and its protonation route," *Struct Chem*, vol. 32, no. 2, pp. 539–551, Apr. 2021, doi: 10.1007/s11224-020-01671-0.

[15] A. D. Becke, "Density-functional exchange-energy approximation with correct asymptotic behavior," *Phys. Rev. A*, vol. 38, no. 6, pp. 3098–3100, Sep. 1988, doi: 10.1103/PhysRevA.38.3098.

[16] A. D. Becke, "Density-functional thermochemistry. I. The effect of the exchange-only gradient correction," *The Journal of chemical physics*, vol. 96, no. 3, pp. 2155–2160, 1992.

[17] M. J. Frisch *et al.*, "Uranyl extraction by N, N-dialkylamide ligands studied by static and dynamic DFT simulations," *Gaussian*, vol. 9, p. 227, 2009.

[18] C. Lee, W. Yang, and R. G. Parr, "Development of the Colle-Salvetti correlation-energy formula into a functional of the electron density," *Phys. Rev. B*, vol. 37, no. 2, pp. 785–789, Jan. 1988, doi: 10.1103/PhysRevB.37.785.

[19] Chr. Møller and M. S. Plesset, "Note on an Approximation Treatment for Many-Electron Systems," *Phys. Rev.*, vol. 46, no. 7, pp. 618–622, Oct. 1934, doi: 10.1103/PhysRev.46.618.

[20] J. R. Durig, G. A. Guirgis, C. Zheng, and T. A. Mohamed, "Spectra and structure of silicon-containing compounds.: Part XXXVIII: Infrared and Raman spectra, vibrational assignment, conformational stability, and ab initio calculations of vinyldifluorosilane," *Spectrochimica Acta Part A: Molecular and Biomolecular Spectroscopy*, vol. 59, no. 9, pp. 2099–2114, 2003.

[21] H. Lampert, W. Mikenda, and A. Karpfen, "Molecular Geometries and Vibrational Spectra of Phenol, Benzaldehyde, and Salicylaldehyde: Experimental versus Quantum Chemical Data," *J. Phys. Chem. A*, vol. 101, no. 12, pp. 2254–2263, Mar. 1997, doi: 10.1021/jp962933g.

[22] A. Nasser, M. A. Migahed, N. M. EL Basiony, H. M. Abd-El-Bary, and T. A. Mohamed, "Raman and Infrared Spectral Analysis, Normal Coordinate Analysis, DFT calculations of Novel Schiff Base Containing di-imine moieties," *Egyptian Journal of Chemistry*, vol. 66, no. 9, pp. 271–291, 2023.

[23] A. Asensio, N. Kobko, and J. J. Dannenberg, "Cooperative Hydrogen-Bonding in Adenine−Thymine and Guanine−Cytosine Base Pairs. Density Functional Theory and Møller−Plesset Molecular Orbital Study," *J. Phys. Chem. A*, vol. 107, no. 33, pp. 6441–6443, Aug. 2003, doi: 10.1021/jp0344646.

[24] D. B. Chesnut and C. G. Phung, "Nuclear magnetic resonance chemical shifts using optimized geometries," *The Journal of chemical physics*, vol. 91, no. 10, pp. 6238–6245, 1989.

[25] V. Chiş, "Molecular and vibrational structure of 2, 4-dinitrophenol: FT-IR, FT-Raman and quantum chemical calculations," *Chemical physics*, vol. 300, no. 1–3, pp. 1–11, 2004.

[26] P. K. Chowdhury, "Infrared depletion spectroscopy of the hydrogen-bonded aniline-diethylamine (C6H5-NH2 center dot center dot center dot NHC4H10) complex produced in supersonic jet," *Journal of Physical Chemistry A*, vol. 107, no. 30, pp. 5692–5696, 2003.

[27] R. Ditchfield, "Self-consistent perturbation theory of diamagnetism: I. A gauge-invariant LCAO method for N.M.R. chemical shifts," *Molecular Physics*, vol. 27, no. 4, pp. 789–807, Apr. 1974, doi: 10.1080/00268977400100711.

[28] H.-G. Korth, M. I. De Heer, and P. Mulder, "A DFT Study on Intramolecular Hydrogen Bonding in 2-Substituted Phenols: Conformations, Enthalpies, and Correlation with Solute Parameters," *J. Phys. Chem. A*, vol. 106, no. 37, pp. 8779–8789, Sep. 2002, doi: 10.1021/jp025713d.

[29] T. Kupka, G. Pasterna, P. Lodowski, and W. Szeja, "GIAO-DFT prediction of accurate NMR parameters in selected glucose derivatives," *Magn. Reson. Chem.*, vol. 37, no. 6, pp. 421–426, Jun. 1999, doi: 10.1002/(SICI)1097-458X(199906)37:6<421::AID-MRC479>3.0.CO;2-W.

[30] T. Kupka, M. Kołaski, G. Pasterna, and K. Ruud, "Towards more reliable prediction of formaldehyde multinuclear NMR parameters and harmonic vibrations in the gas phase and solution," *Journal of Molecular Structure: THEOCHEM*, vol. 467, no. 1, pp. 63–78, 1999.

[31] V. G. Malkin, O. L. Malkina, M. E. Casida, and D. R. Salahub, "Nuclear Magnetic Resonance Shielding Tensors Calculated with a Sum-over-States Density Functional Perturbation Theory," *J. Am. Chem. Soc.*, vol. 116, no. 13, pp. 5898–5908, Jun. 1994, doi: 10.1021/ja00092a046.

[32] W. J. Hehre, "Ab initio molecular orbital theory," *Acc. Chem. Res.*, vol. 9, no. 11, pp. 399–406, Nov. 1976, doi: 10.1021/ar50107a003.

[33] T. A. Mohamed, U. A. Soliman, A. I. Hanafy, and A. M. Hassan, "Conformational stability, barriers to internal rotation of 2-aminothiophenol (d0 and d3): A combined vibrational and theoretical approach," *Journal of Molecular Structure: THEOCHEM*, vol. 865, no. 1–3, pp. 14–24, 2008.

[34] T. A. Mohamed, I. A. Shabaan, W. M. Zoghaib, J. Husband, R. S. Farag, and A. E.-N. M. Alajhaz, "Tautomerism, normal coordinate analysis, vibrational assignments, calculated IR, Raman and NMR spectra of adenine," *Journal of Molecular Structure*, vol. 938, no. 1–3, pp. 263–276, 2009.

[35] U. A. Soliman, A. M. Hassan, and T. A. Mohamed, "Conformational stability, vibrational assignmenents, barriers to internal rotations and ab initio calculations of 2-aminophenol (d0 and d3)," *Spectrochimica Acta Part A: Molecular and Biomolecular Spectroscopy*, vol. 68, no. 3, pp. 688–700, 2007.

[36] S. M. Hassan, H. A. Emam, and M. M. Abdelall, "Heteroaromatization with Ketene Dithioacetals: Part II. Synthesis of Some Novel 5-Aminopyrazole-3-Carbonitrile, 3-Carboxamide and Pyrazolo [3, 4-d] Pyrimidin-4-One Derivatives as Antimicrobial Agents," *Phosphorus, Sulfur, and Silicon and the Related Elements*, vol. 175, no. 1, pp. 109–127, 2001.

[37] P. Pulay, "Ab initio calculation of force constants and equilibrium geometries in polyatomic molecules: I. Theory," *Molecular Physics*, vol. 17, no. 2, pp. 197–204, 1969.

[38] J. Zukerman-Schpector, E. J. Barreiro, and A. C. C. Freitas, "Structures of pyrazole derivatives. III. 5-Amino-4-cyano-1-phenylpyrazole," *Acta Crystallographica Section C: Crystal Structure Communications*, vol. 50, no. 12, pp. 2095–2096, 1994.

[39] P. Prusiner, M. Sundaralingam, T. Ito, and T. Sakurai, "The crystal and molecular structure of 3-amino-4, 5-dicyano-1-methylpyrazole," *Acta Crystallographica Section B: Structural Crystallography and Crystal Chemistry*, vol. 32, no. 3, pp. 853–856, 1976.

[40] J. Zukerman-Schpector, E. E. Castellano, G. Oliva, A. C. Massabni, and A. D. Pinto, "Hydrogen bonding in the crystal structures of the adducts between 1-phenyl-3, 5-dimethylpyrazole with oxalic and perchloric acids," *Canadian Journal of Chemistry*, vol. 62, no. 4, pp. 725–728, 1984.

[41] A. van Bondi, "van der Waals volumes and radii," *The Journal of physical chemistry*, vol. 68, no. 3, pp. 441–451, 1964.

[42] J. E. Huheey, E. A. Keiter, R. L. Keiter, and O. K. Medhi, *Inorganic chemistry: principles of structure and reactivity*. Pearson Education India, 2006.

[43] H. Lampert, W. Mikenda, and A. Karpfen, "Molecular geometries and vibrational spectra of phenol, benzaldehyde, and salicylaldehyde: experimental versus quantum chemical data," *The Journal of Physical Chemistry A*, vol. 101, no. 12, pp. 2254–2263, 1997.

[44] T. A. Mohamed, G. A. Guirgis, Y. E. Nashed, and J. R. Durig, "Spectra and structure of silicon containing compounds: Part XXXIV. Raman and infrared spectra, vibrational assignment, barriers to internal rotation, and ab initio calculations of 1-chloroethylsilane," *Vibrational spectroscopy*, vol. 30, no. 2, pp. 111–120, 2002.

[45] T. Kupka, G. Pasterna, P. Lodowski, and W. Szeja, "GIAO-DFT prediction of accurate NMR parameters in selected glucose derivatives," *Magn. Reson. Chem.*, vol. 37, no. 6, pp. 421–426, Jun. 1999, doi: 10.1002/(SICI)1097-458X(199906)37:6<421::AID-MRC479>3.0.CO;2-W.

[46] V. Barone, M. Cossi, and J. Tomasi, "A new definition of cavities for the computation of solvation free energies by the polarizable continuum model," *The Journal of chemical physics*, vol. 107, no. 8, pp. 3210–3221, 1997.

[47] J. Tomasi and M. Persico, "Molecular interactions in solution: an overview of methods based on continuous distributions of the solvent," *Chemical Reviews*, vol. 94, no. 7, pp. 2027–2094, 1994.

[48] L. J. Bellamy and R. L. Williams, "The NH stretching frequencies of primary amines," *Spectrochimica Acta*, vol. 9, no. 4, pp. 341–345, 1957.

[49] J. Swaminathan, M. Ramalingam, and N. Sundaraganesan, "Molecular structure and vibrational spectra of 3-amino-5-hydroxypyrazole by density functional method," *Spectrochimica Acta Part A: Molecular and Biomolecular Spectroscopy*, vol. 71, no. 5, pp. 1776–1782, 2009.

[50] T. A. Mohamed, "Structural parameters, barriers to internal rotation, normal coordinate analysis and quantum mechanics calculations of 1, 1, 1-trimethyldisilane," *Journal of Molecular Structure: THEOCHEM*, vol. 635, no. 1–3, pp. 161–172, 2003.

[51] T. A. Mohamed and M. M. Abo Aly, "Vibrational analysis, conformational stability, force constants, barriers to internal rotations, RHF, MP2 and DFT calculations of trans, trans-2, 4-hexadiene," *Journal of Raman Spectroscopy*, vol. 35, no. 10, pp. 869–878, 2004.

[52] T. A. Mohamed and R. S. Farag, "Raman spectrum, conformational stability, barriers to internal rotations and DFT calculations of 1, 1, 1-trifluoro-propane-2-thione with double-internal-symmetric rotor," *Spectrochimica Acta Part A: Molecular and Biomolecular Spectroscopy*, vol. 62, no. 4–5, pp. 800–807, 2005.

[53] J. R. Durig, G. A. Guirgis, and S. Bell, "Torsional spectrum and ab initio calculations for propene," *The Journal of Physical Chemistry*, vol. 93, no. 9, pp. 3487–3491, 1989.

[54] J. R. Durig, W. J. Natter, and P. Groner, "Analysis of torsional spectra of molecules with two internal C 3 V rotors. IX. The torsional potential functions of isobutene-d and-d 6," *The Journal of Chemical Physics*, vol. 67, no. 11, pp. 4948–4951, 1977.

[55] R. t Schwendeman and G. D. Jacobs, "Molecular structure of ethyl chloride," *The Journal of Chemical Physics*, vol. 36, no. 5, pp. 1245–1250, 1962.